International Journal of Innovation and Industrial Revolution
IJIREV
EISSN: 2637-0972
Volume 7 Issue 23 (December 2025) PP. 568-592
DOI 10.35631/IJIREV.723038

INTERNATIONAL JOURNAL OF INNOVATION AND INDUSTRIAL REVOLUTION (IJIREV)
www.ijirev.com

A COMPARATIVE STUDY OF DIFFERENT THRESHOLDING TECHNIQUES IN SEGMENTING POROUS GALLIUM NITRIDE IN FIELD EMISSION SCANNING ELECTRON MICROSCOPY IMAGE

Syed Taufiq Akmal Syed Nasiruddin[1], Ainorkhilah Mahmood[2*], Adi Izhar Che Ani[3], Mohd Firdaus Abdullah[4], Nur Maizatul Azra Mukhtar[5], Naser Mahmoud Ahmed[6], Nur Iwani Nor Izaham[7]

[1] Department of Applied Sciences Universiti Teknologi MARA Cawangan Pulau Pinang, 13500 Permatang Pauh, Penang, Malaysia
Email: 2024122641@student.uitm.edu.my
[2] Department of Applied Sciences Universiti Teknologi MARA Cawangan Pulau Pinang, 13500 Permatang Pauh, Penang, Malaysia
Email: ainorkhilah_sp@uitm.edu.my
[3] Centre for Electrical Engineering Studies, Universiti Teknologi MARA Cawangan Pulau Pinang, 13500 Permatang Pauh, Penang, Malaysia
Email: adiizhar@uitm.edu.my
[4] Centre for Electrical Engineering Studies, Universiti Teknologi MARACawangan Pulau Pinang, 13500 Permatang Pauh, Penang, Malaysia
Email: f.abdullah@uitm.edu.my
[5] Faculty of Health Sciences, Universiti Teknologi MARA Cawangan Pulau Pinang, 13200 Kepala Batas, Penang, Malaysia
Email: mnurmaizatul038@uitm.edu.my
[6] Laser and Optoelectronics Engineering Department, Dijlah University College, 00964 Baghdad, Iraq
Email: naser.mahmoud@duc.edu.iq
[7] Faculty of Applied Sciences, Universiti Teknologi MARA, 40450 Shah Alam, Selangor, Malaysia
Email: nuriwani1999@gmail.com
[*] Corresponding Author

Article Info:

Article history:
Received date: 26.10.2025
Revised date: 09.11.2025
Accepted date: 18.12.2025
Published date: 31.12.2025

Abstract:

The quantitative analysis of porous gallium nitride (GaN) nanostructures is critical for understanding the optoelectronic properties and engineering the bandgap of photodetector devices. Yet, this task remains a challenge due to the complexity of pore morphology and the limitations of conventional image processing approaches in segmenting the porous region. In this study, field emission scanning electron microscopy (FESEM) images of photoelectrochemically etched GaN samples were examined to assess the effectiveness of different thresholding methods on segmenting the porous

International Journal of Innovation and Industrial Revolution
IJIREV
EISSN: 2637-0972
Volume 7 Issue 23 (December 2025) PP. 568-592
DOI 10.35631/IJIREV.723038

To cite this document:

Syed Nasiruddin, S. T. A., Mahmood, A., Che Ani, A. I., Abdullah, M. F., Mukhtar, N. M. A., Ahmed, N. M., & Nor Izaham, N. I. (2025). A Comparative Study of Different Thresholding Techniques in Segmenting Porous Gallium Nitride in Field Emission Scanning Electron Microscopy Image. *International Journal of Innovation and Industrial Revolution, 7* (23), 568-592.

DOI: 10.35631/IJIREV.723038

This work is licensed under CC BY 4.0

region by estimating the porous parameter. The thresholding under study are Otsu thresholding, manual thresholding, and adaptive thresholding. These methods were evaluated across multiple magnifications and etching durations to estimate their porosity and average pore diameter. The results indicate that manual thresholding achieved porosity errors as low as 17.87% in shorter etching samples, while Otsu's thresholding yielded errors as low as 24.32% in longer porous samples. For average pore diameter estimation, manual thresholding similarly performed best at short etching durations with a 32.13% error, whereas Otsu's thresholding was optimal for longer etching durations with only 2.76% errors. Regardless, the selection of the optimal thresholding method across different magnifications proved challenging, as no consistent pattern was observed. However, among the reliable estimates across magnification, most were found in 25kx and 50kx magnification images. Whereby at these two magnifications, many estimate produce a lower percentage error estimate of less than 20% compared to higher magnification images. This study further highlights the limitations of pixel intensity-based segmentation methods and the need for more advanced approaches for accurate quantification of porous GaN nanostructures.

Keywords:

Etching, Gallium Nitride, Image Processing, Morphology, Porous, Pore Size, Thresholding

Introduction

The efforts of photonic researchers in band-gap engineering through nano-structuring the surface of semiconductors, especially GaN for photodetector applications have been intensified. Among the nanostructures, nanoporous has been shown to demonstrate high detectability, high sensitivity and the fastest photo-response speed in comparison to other implemented morphologies on GaN UV photodetectors (Hu et al., 2023). It has been noted that the porous nanostructure produced through the etching process has a direct influence on the optoelectronic properties of a semiconductor (Abdul Amir et al., 2021; Abdulkhaleq et al., 2020; Li et al., 2023; Son et al., 2022). The influence of porosity on the performance of photodetectors is evident, suggesting a necessary role in tailoring the performance and characteristics suitable for photodetector devices. Regardless, extensive research is needed to precisely fine-tune and understand the effects of porosity on both optical and electrical properties.

There have been several methodological studies reported to create a porous structure on the surface of GaN for photodetector devices. Among the favorable methods is through wet etching due to its low cost and ability to precisely control the pore morphology (Abbas & Kadhm, 2024; Khudiar et al., 2022; Kuntyi et al., 2022). Additionally, the method has been demonstrated to maintain a consistent crystal quality compared to dry etching which has been reported to induce surface damage and disturb the lattice arrangement causing increased leakage current and reduced reliability of the device (Cui et al., 2021; Ge et al., 2022; Meyers et al., 2020). The use of high-kinetic plasma to remove semiconductor atoms and produce voids on the semiconductor surface through a complex setup is known to be non-economic (Taufiq et al., 2025). Consequently, these factors contributed to less favorability in employing the dry etching.

International Journal of Innovation and Industrial Revolution
IJIREV
EISSN: 2637-0972
Volume 7 Issue 23 (December 2025) PP. 568-592
DOI 10.35631/IJIREV.723038

Photoelectrochemical etching (PECE) was among the wet etching methods as shown in **Figure 1 (b)** that has gained considerable attention for suitability in fabricating porous structures (Son et al., 2022). Unlike normal electrochemical etching, PECE creates high-quality pore formation through the combination of light illumination and an applied bias. This technique is comparatively simple and often carried out by immersing the GaN film in an etching solution or electrolyte, where the surface atoms are removed through chemical reactions with the assistance of UV light to overcome the wide bandgap of GaN and generate electron-hole pairs at the semiconductor-electrolyte interface (Meyers et al., 2020; Son et al., 2022). The photogenerated holes at the GaN surface drive the oxidation of GaN, which subsequently dissolves in the electrolyte, leading to the formation of porous structures (Trichas et al., 2008). Furthermore, the process minimizes damages to the crystal surface compared to dry etching methods making it highly suitable for tailoring porosity in GaN for applications such as optoelectronic devices, sensors and energy conversion systems (Meyers et al., 2020).

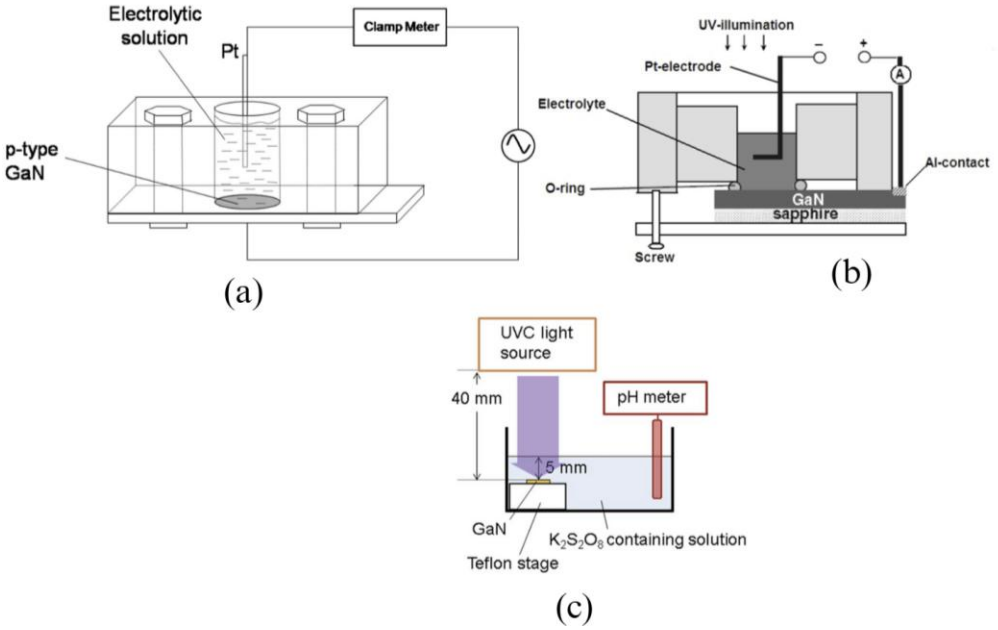

Figure 1: Several Wet Etching Techniques (A) Electrochemical Etching (Quah Et Al., 2016) (B) Photoelectrochemical Etching (Al-Heuseen & Alquran, 2018) And (C) Electroless Etching (Toguchi Et Al., 2019)

The characterization of surface morphology in porous GaN remains a challenge despite porous GaN having been widely fabricated and investigated for its potential in optoelectronic and sensing applications. The irregularity and complexity of pore morphologies make the analysis difficult to obtain consistent and reliable by image processing (Fauzi et al., 2023; Isa et al., 2022). Conventional surface analysis methods, particularly threshold-based image processing of FESEM images are highly sensitive to parameter selection and often yield inconsistent results. This lack of standardized evaluation hinders a deeper understanding and comparison of porous GaN structures across studies.

In image processing, determining the correct threshold value to represent the porous regions in an image is often challenging due to the complex nature of porous structures. The segmentation process must accurately distinguish the porous region, which is complicated because of the smooth contrast transition or multilevel pixel intensity within the nanostructure (Fauzi et al.,

International Journal of Innovation and Industrial Revolution
IJIREV
EISSN: 2637-0972
Volume 7 Issue 23 (December 2025) PP. 568-592
DOI 10.35631/IJIREV.723038

2023). This involves converting a grayscale image into a binary image by separating pixel values into two groups: black pixels (background, surface) and white pixels (foreground, porous). Otsu's global thresholding technique uses a single threshold value to segment the overall image into the background or foreground. The algorithm selects the optimum class variance to compute the threshold value (Cao et al., 2021). Otsu's thresholding is particularly effective when the image's histogram has a bimodal distribution. Its simplicity and computational efficiency make it a popular choice for many applications, including document binarization, medical image analysis and object recognition in computer vision (Muhamad Rizal et al., 2014). Meanwhile, adaptive thresholding is a local thresholding method that uses the local mean intensity (first-order statistics) in the neighborhood of each pixel to determine the threshold value. The thresholding value in the adaptive thresholding is computed based on the local mean relative to the intensity pixel surrounding the preset size sliding square window that moves throughout the image. Unlike Otsu's thresholding, the adaptive thresholding can adapt to various contrasts and illumination of the images that differ in intensity level across different regions of the image (Raheem & Shabat, 2023).

For the image processing of porous GaN, the analysis remains unclear whether previous studies have explicitly employed global or local thresholding techniques. However, evidence from prior work (Isa et al., 2022) suggests the use of a predetermined global threshold to define the pixel separation value during segmentation. As illustrated in **Figure 2**, a normalized pixel intensity threshold of approximately 0.2 has been applied to distinguish the porous regions from the surface structure. Since no systematic comparison between different thresholding approaches has been carried out, this study explores global, manual and adaptive methods to evaluate their suitability for quantifying porous parameters. This comparative analysis provides insight into the strengths and limitations of threshold-based segmentation in the characterization of porous GaN.

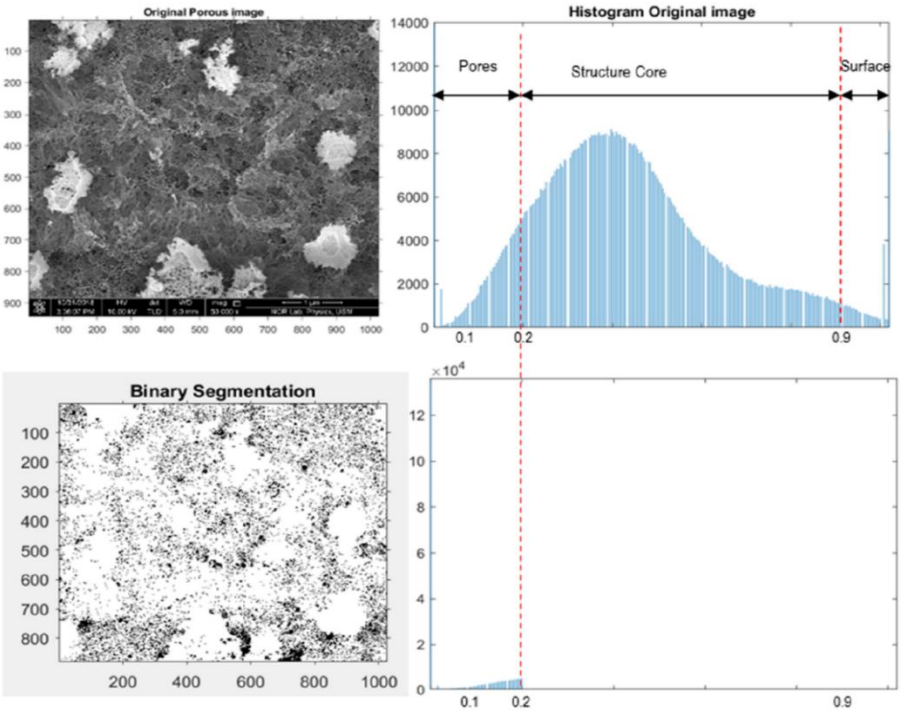

Figure 2: Manual Thresholding In Separating The Porous Structure
Source: Courtesy of (Isa et al., 2022)

International Journal of Innovation and Industrial Revolution
IJIREV
EISSN: 2637-0972
Volume 7 Issue 23 (December 2025) PP. 568-592
DOI 10.35631/IJIREV.723038

Literature Review

The application of image processing techniques for determining porous parameters has been widely reported in the literature, particularly in studies utilizing wet etching methods to fabricate porous nanostructures. Ahmad et al. (2012) applied image processing techniques in MATLAB to perform binary conversion of images through thresholding allowing distinct segmentation between porous regions (foreground) and surface regions (background). The study demonstrated that increasing the current density during electrochemical etching using a mixed electrolyte of ethanol: hydrofluoric acid (HF) ratio of 5:1 from 50 mA/cm² to 75 mA/cm² enhanced the porosity from 24% to 51%, while simultaneously expanding the pore diameter distribution from 250-400 nm to 600-3500 nm range. A Wiener2 filter was also employed to suppress noise in the 50kx magnification SEM images prior to binarization. Building upon this work, Mahmood et al. (2014) adopted a similar image processing approach in 50kx SEM images and reported increased porosity through photoelectrochemical etching using a 500 W UV light source. By varying the current density from 20 mA/cm² to 60 mA/cm² under a 3% KOH electrolyte, the study observed porosity improvements from 30.6% to 43.2% with the highest-porosity sample exhibiting a dominant pore diameter of 256.54 nm. Elia et al.(2016) were among the first to employ the FESEM instrument through model JEOL JSM 7400F to analyze porous structures fabricated through electrochemical etching in an HF/ethanol etching solution, focusing on the effect of varying current densities. The study uses a fixed magnification of 300kx for the FESEM images and morphological filtering was applied to eliminate small closed shapes embedded within the porous structures. A minimum size of 21 pixels was set to remove isolated features, while thresholding was performed using an iterative bisection histogram method. From the binarized images, several pore characteristics were quantified with a more transparent feature extraction, which included area, perimeter and the shortest/longest pore dimensions. Furthermore, the study also employed multiple feature descriptors to characterize the porous parameters by combining the measurements to represent the average pore diameter. When the current density was raised from 4 mA/cm² to 45 mA/cm² under a 25% HF electrolyte, porosity increased from 36% to 42% and the average pore diameter grew from 9.2 nm to 16.9 nm. These findings confirm the direct influence of current density on enhancing porosity and enlarging pore dimensions. The studies by Isa et al.(2022) and Fauzi et al.(2023) employed manual thresholding by setting the pixel intensity threshold at approximately 0.2. The FESEM magnifications considered in both works included 50kx, 100kx and 200kx. Feature extraction was explicitly described with parameters such as area, major axis and minor axis used to quantify porosity and pore diameter. In addition, both studies combined FESEM analysis with atomic force microscopy to correlate the surface morphology with the depth of the porous structure. **Table 1** summarizes the related research on investigating the morphological structure of porous GaN through image processing.

Table 1: Summary Of Image Processing Approaches for Porous Gan Characterization

Author	Image Acquisition	Magnification	Preprocessing	Segmentation	Feature Extraction	Measurement
Ahmed et al., 2012	SEM	50kx	Grayscale, noise removal	Boundary tracing, binarize	Area, diameter	Porosity, pore diameter
Mahmood et al., 2014	SEM	50kx	Grayscale, noise removal	Boundary tracing, binarize	Area, diameter	Porosity, pore diameter

International Journal of Innovation and Industrial Revolution
IJIREV
EISSN: 2637-0972
Volume 7 Issue 23 (December 2025) PP. 568-592
DOI 10.35631/IJIREV.723038

Elia et al., 2016)	FESEM	300kx	Morphological filter	Binarize, iterative bisection histogram	Area, perimeter, shortest and longest length	Average diameter, porosity
(Isa et al., 2022)	FESEM	50kx, 100kx and 200kx	Grayscale, noise removal	Manual thresholding	Greyscale intensity, area, major axis length and minor axis length	Porosity, pore diameter, pore depth, surface roughness
Fauzi et al., 2023	FESEM	50kx, 100kx and 200kx	Grayscale, noise removal	Manual thresholding	Greyscale intensity, area	Pore depth, pore diameter

While these studies demonstrate the effectiveness of image processing in quantifying porous GaN structures, the image processing largely relies on single thresholding strategies without systematic comparison. Thresholding is often implemented as a fixed or manually set value with limited justification for its selection. This raises questions about reproducibility and consistency across magnifications or etching conditions. Moreover, most works emphasize the role of etching parameters in determining porosity while the influence of image analysis methodology itself remains underexplored. To address these gaps, the present study investigates the performance of global, manual and adaptive thresholding methods applied across multiple magnifications and etching durations, thereby providing a clearer perspective on how thresholding choice affects the quantification of porous parameters.

Materials and Methods

By referring to **Figure 3**, the study consists of six important steps: sample and image acquisition, image preprocessing, applying various thresholding techniques, image post-processing, feature extraction and quantification, and finally comparative evaluation. The following paragraph explains each step in detail.

Samples and Image Acquisition

In the first step, four samples of undoped GaN denoted as U45, U60, U75 and U90 were etched according to the etching duration represented by the respective suffixes. The etching of the samples was prepared under a fixed anodization current of 100 mA and illuminated under a 400 W mercury high-pressure vapor lamp to enhance the PECE process and facilitate the formation of porous structures. The variation in etching duration was intended to induce differences in pore morphology and enable comparative analysis of structural examination. The 20 raw FESEM images of fabricated porous GaN from the study by Izaham et al. (2024) were captured using an advanced electron microscopy instrument, FESEM (Model FEI Verios 460L) located at the Science & Engineering Research Centre (SERC), Universiti Sains Malaysia, Nibong Tebal, Pulau Pinang, Malaysia. The images were saved in Tagged Image File Format, commonly known as TIFF with a dimension of 1103 × 1536 × 3 and a data class of uint8. Each image of the porous GaN sample was acquired under different magnifications of 25kx, 50kx, 100kx, 200kx and 250kx. **Table 2** and **Table 3** convey the distributions of each respective visual image used for the study at five stated distinct magnifications.

International Journal of Innovation and Industrial Revolution
IJIREV
EISSN: 2637-0972
Volume 7 Issue 23 (December 2025) PP. 568-592
DOI 10.35631/IJIREV.723038

Table 2: Gan Sample Of FESEM Images

Etching Duration (min)	Magnification Level				
	25kx	50kx	100kx	200kx	250kx
45	1	1	1	1	1
60	1	1	1	1	1
75	1	1	1	1	1
90	1	1	1	1	1
Total images	20				

Table 3: FESEM Images At Different Magnifications

Etching Duration (min)	Magnification Level				
	25kx	50kx	100kx	200kx	250kx
45	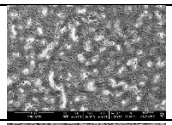	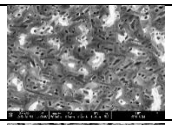	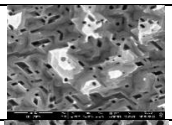	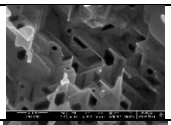	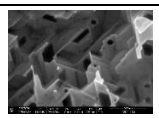
60	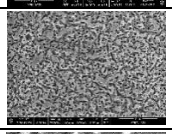	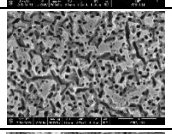	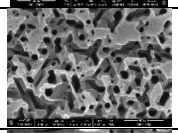	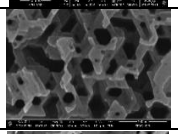	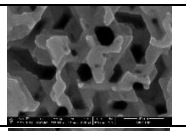
75	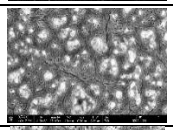	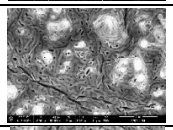	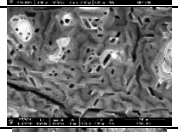	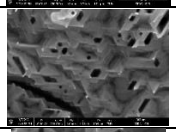	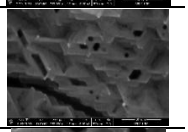
90	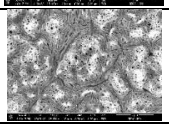	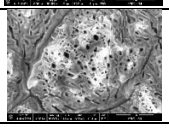	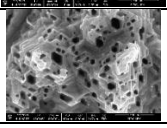	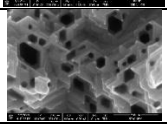	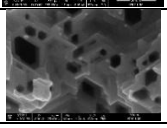
Total images	20				

International Journal of Innovation and Industrial Revolution
IJIREV
EISSN: 2637-0972
Volume 7 Issue 23 (December 2025) PP. 568-592
DOI 10.35631/IJIREV.723038

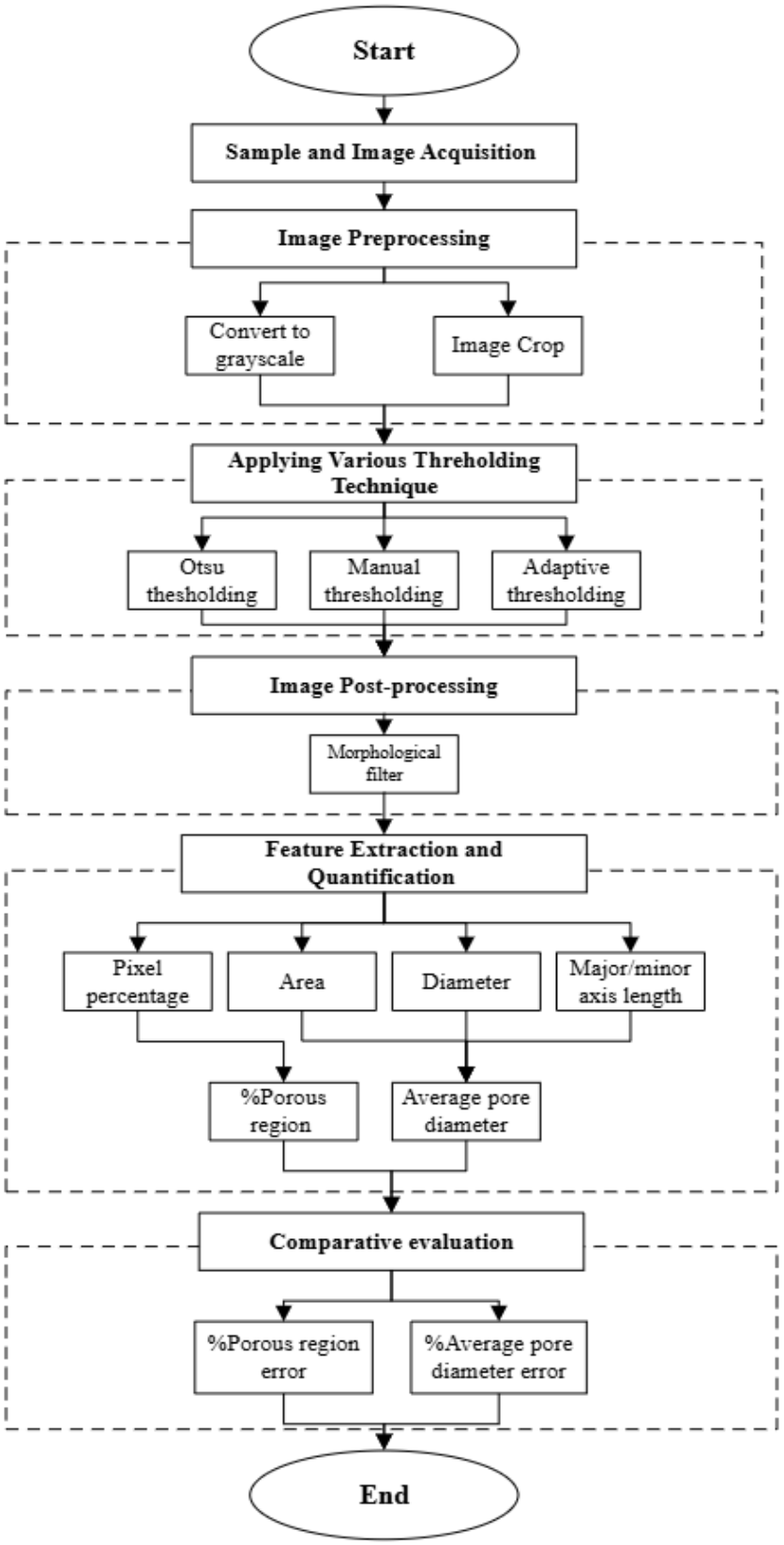

Figure 3: Flowchart of Comparative Thresholding Study

International Journal of Innovation and Industrial Revolution
IJIREV
EISSN: 2637-0972
Volume 7 Issue 23 (December 2025) PP. 568-592
DOI 10.35631/IJIREV.723038

Image Preprocessing

In the image preprocessing step, all the raw FESEM images are converted from a three-channel image into a single-channel image. The subheader that contains the details regarding the scale length, date and other information as shown in Figure 4, was cropped out. The measurement of the length scale of each magnification was noted and will be used in the pixel length to physical length conversion. Additionally, due to the complexity of the porous region in preparing the manual polygon annotation of the ground truth mask, the images are then further cropped into four quadrants with an equal size of 817 × 567 pixels as shown in Figure 5. Out of the four images produced, one was selected randomly to represent the sample at that magnification. This procedure was important to reduce the amount of complex annotation in preparing the ground truth data for the segmentation.

Figure 4: The Cropped Subheader Contains Information Regarding the Length Scale (Shown in the Blue Rectangle)

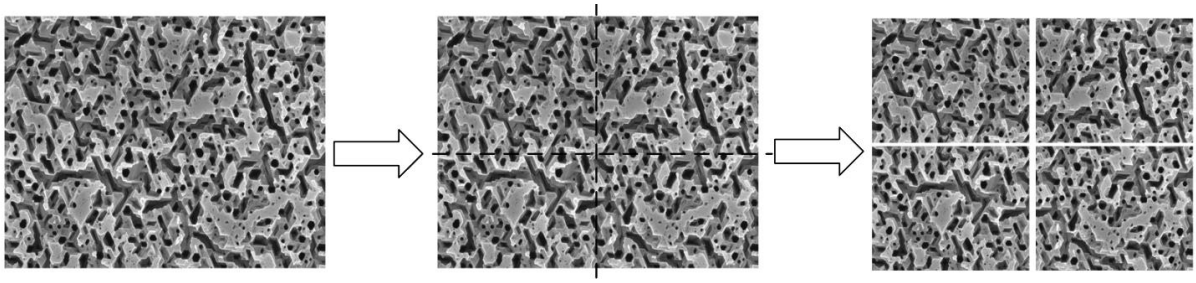

Figure 5: Image Cropped into Four Regions and One Selected Randomly to Represent the Image

Manual Annotation of Segmentation Region

The ground truth segmentation mask of the respective cropped image was prepared using Roboflow, a computer vision platform commonly employed for developing and deploying computer vision models. In the application, polygon annotations were used to label each porous region on the cropped image. These polygon annotations of each represented magnification are then converted into a polygon mask, where the foreground region represents the porous structure, while the background refers to the surface region. The process of converting the polygon segmentation point into the polygon mask was shown in **Figure 6**. Whereby in the process, the use of metadata exported from the Roboflow was transformed from a 1-dimensional data point into a 2-dimensional data point that can represent the porous region on the image. The process was done on MATLAB software. The produced masks are then validated by two experts in the field of porous GaN and image processing to verify the validity of the segmented region.

International Journal of Innovation and Industrial Revolution
IJIREV
EISSN: 2637-0972
Volume 7 Issue 23 (December 2025) PP. 568-592
DOI 10.35631/IJIREV.723038

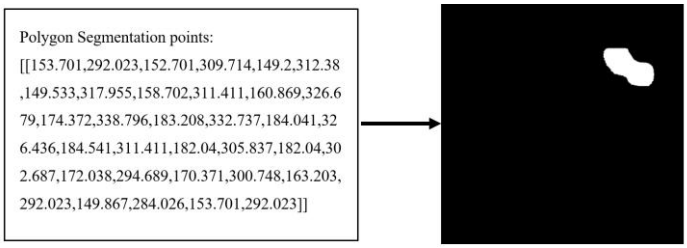

Figure 6: Image Conversion of Polygon Datapoint into Porous Segmentation Region.

Applying Various Thresholding Techniques

Different thresholding techniques are applied to the grayscale image to segment the porous structure into foreground and background regions creating a binary image. The result of the binary image $I_{BW}(x, y)$ was determined from the pixel intensity of the grayscale image $I_G(x, y)$ whereas if the value of the grayscale pixel exceeds the threshold value, the binary intensity of 1 is allocated to that pixel corresponding to the foreground regions. If the grayscale pixel intensity is equal to or below the threshold value, the binary intensity of 0 is allocated to that pixel. The thresholding of pixels into binary 0 and 1 is shown in **Eq. (1)** (Hussain et al., 2024).

$$I_{BW}(x,y) = \begin{cases} 1 \; if \; I_G(x,y) > threshold \\ 0 \; if \; I_G(x,y) \leq threshold \end{cases} \quad (1)$$

The threshold methods employed to determine the threshold values include Otsu's thresholding, manual thresholding and Adaptive thresholding. In Otsu's thresholding, functions *otsuthresh* and *imbinarize* are used to segment the pixels into foreground and background. The threshold is based on maximizing inter-class variance in an image grayscale intensity histogram to find the optimal global threshold value. While the manual thresholding was referred to study by Isa et al.(2022) where a normalized pixel intensity value of less than 0.2 was used to represent the porous threshold. In adaptive thresholding, the threshold value used to segment the pixels was determined from a sliding window of approximately 51 × 35 pixels (corresponding to the default neighborhood size of image size/16 in MATLAB (version R2024a). Since adaptive thresholding is a local thresholding, the threshold values are not fixed across all the regions within the same image. Each thresholding technique is applied separately to a single image and the resulting images are shown in the **Table. 4**.

Image Postprocessing

In the image postprocessing stage, an additional simple refinement was carried out across all the outputs of the thresholding images to improve the accuracy of the pore segmentation. The method follows the study by Elia et al. (2016) whereby a morphological filtering step through the specific MATLAB function *bwareaopen* was applied to remove isolated porous regions below a specified size. Only the pores with a connected component smaller than 21 pixels in area were eliminated in the binary mask.

International Journal of Innovation and Industrial Revolution
IJIREV
EISSN: 2637-0972
Volume 7 Issue 23 (December 2025) PP. 568-592
DOI 10.35631/IJIREV.723038

Table 4: Result Of Threshold Image And Ground Truth Images Across All Samples And Magnification

Sample	Magnification	Image	Ground Truth	Otsu Thresholding	Manual Thresholding	Adaptive Thresholding
U45	25kx	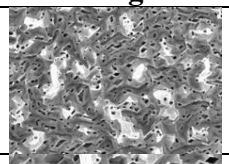		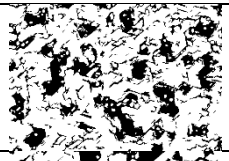		
	50kx	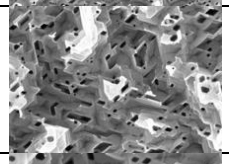		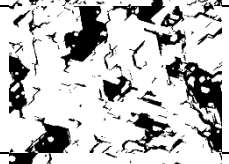		
	100kx	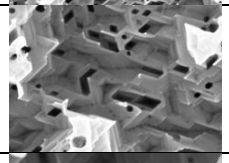				
	200kx	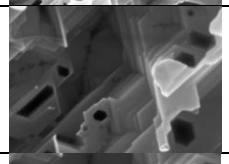	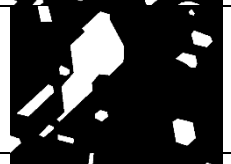			
	250kx	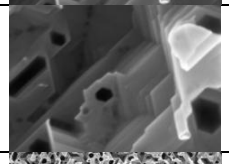				
U60	25kx	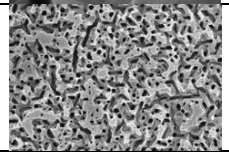	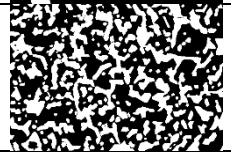	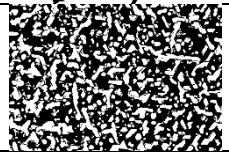	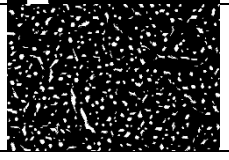	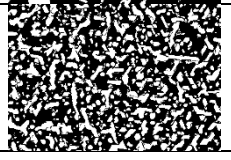

International Journal of Innovation and Industrial Revolution
IJIREV
EISSN: 2637-0972
Volume 7 Issue 23 (December 2025) PP. 568-592
DOI 10.35631/IJIREV.723038

	50kx	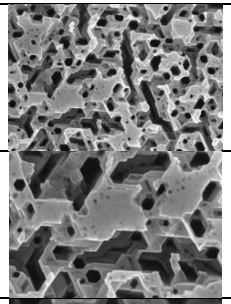	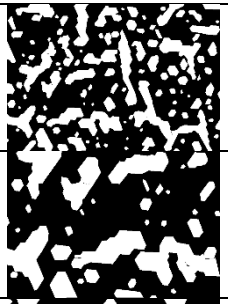	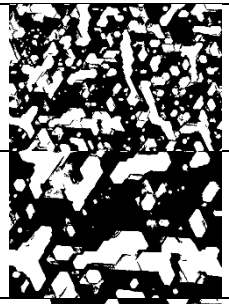		
	100kx					
	200kx	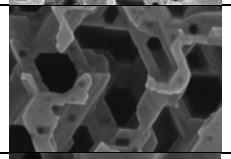				
	250kx	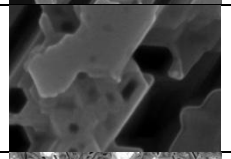				
U75	25kx	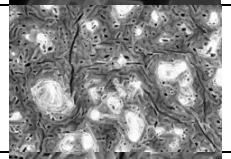		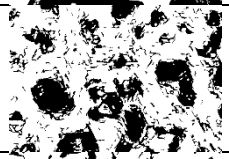		
	50kx	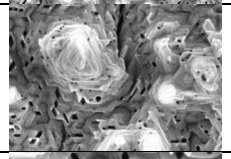				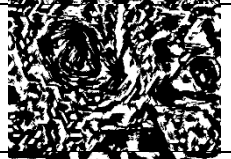
	100kx	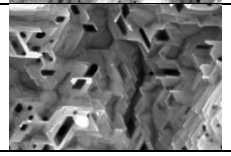	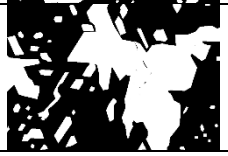			

International Journal of Innovation and Industrial Revolution
IJIREV
EISSN: 2637-0972
Volume 7 Issue 23 (December 2025) PP. 568-592
DOI 10.35631/IJIREV.723038

	200kx	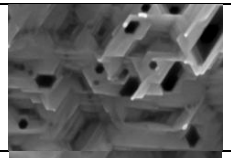				
	250kx	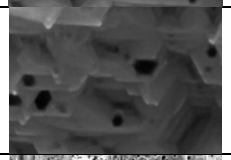			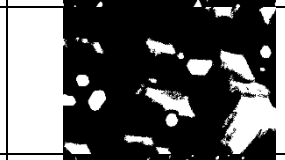	
U90	25kx	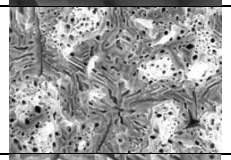		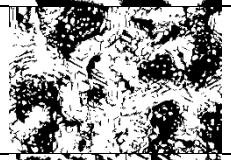	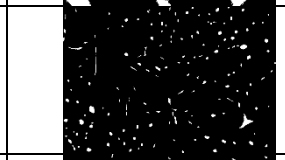	
	50kx	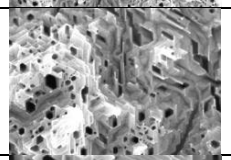		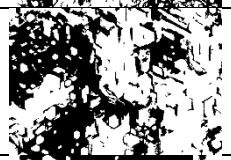		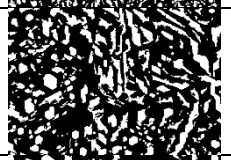
	100kx	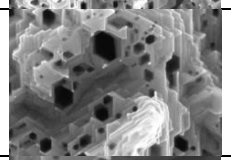		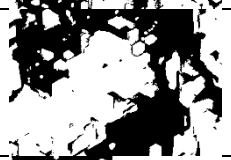	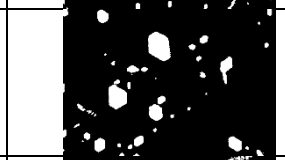	
	200kx	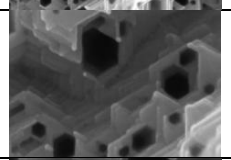				
	250kx	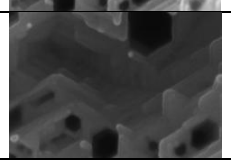			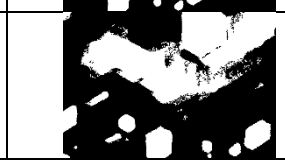	

International Journal of Innovation and Industrial Revolution
IJIREV
EISSN: 2637-0972
Volume 7 Issue 23 (December 2025) PP. 568-593
DOI 10.35631/IJIREV.723038

Feature Extraction and Quantification

As shown in **Figure 7**, the extracted features from the foreground region in each segmented image are area, major axis length (Lx), minor axis length (Ly) and equivalent diameter. Through the Region Analyzer tool in MATLAB, the measurement for the quantification of porous parameter was derived.

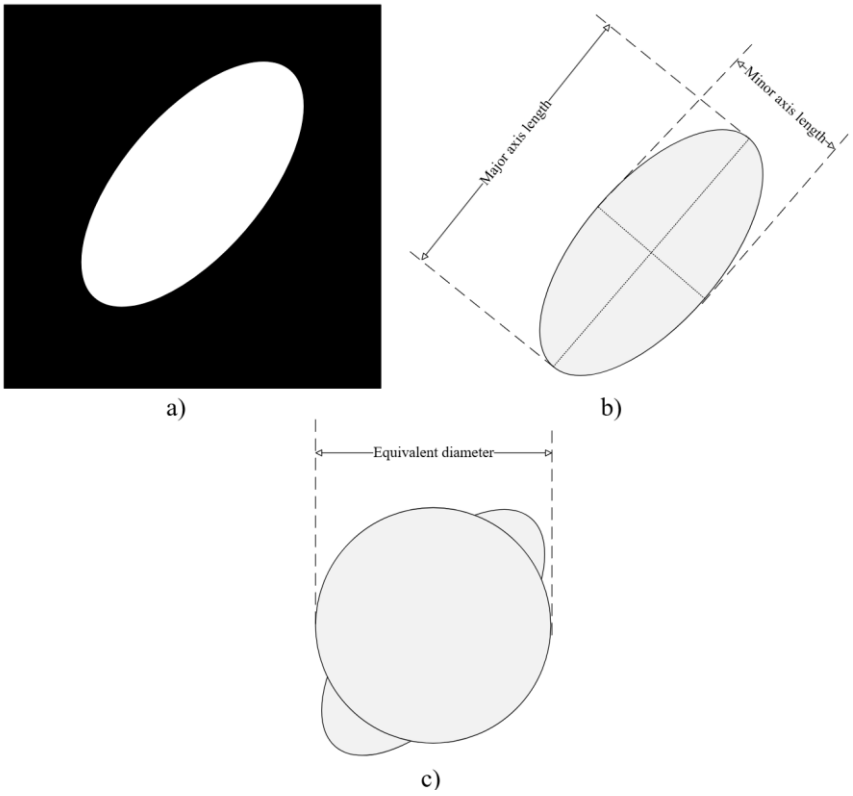

Figure 7: Feature Extraction Of (A) Foreground Region into Quantified (B) Major/Minor Axis Length And (C) Diameter

For the foreground percentage of the porous region, the study adopted the approach of Isa et al.(2022) whereby the binary segmentation masks were quantified by computing the ratio of the pore area that corresponds to the foreground pixels to the total sample area that corresponds to the resolution of the image. The equation to measure the porosity was shown in **Eq. (2).**

$$Porosity\ (\%) = \frac{Total\ \text{pore area}}{Total\ area} \times 100\% \qquad (2)$$

While the average pore diameter was measured through combined descriptors of Lx, Ly and area (assuming circular shape) as shown in **Eq. (3)** and **Eq. (4),** respectively. The study implemented a method demonstrated by Elia et al.(2016) through the use of multiple feature descriptors to provide a better estimate of both the pore elongation and orientation (major/minor axis lengths) at the same time, considering the area of that pore region (equivalent diameter). The i in both equations refers to the individual pores in the mask image. Each

International Journal of Innovation and Industrial Revolution
IJIREV
EISSN: 2637-0972
Volume 7 Issue 23 (December 2025) PP. 568-593
DOI 10.35631/IJIREV.723038

respective pixel length was then converted into physical length provided through the scale bar in each of the original raw FESEM images.

$$average\ pore\ diameter\ = \frac{\sum_{i=1}^{n} \frac{L_{x_i} + L_{y_i}}{2}}{n} \quad \textbf{(3)}$$

$$average\ pore\ diameter, (2r)\ = \frac{\sum_{i=1}^{n} \sqrt{\frac{Area_i}{\pi}}}{n} \quad \textbf{(4)}$$

Performance Evaluation

The measured quantities of porosity and average pore diameter were compared against the ground truth measurements. In measuring the percentage region error and percentage pore diameter error, the measurements from the threshold values were compared with the ground truth values as shown in **Eq. (5)**. Whereby the threshold value refers to the quantities of the porosity and average pore diameter, while the ground truth values are derived from the polygon mask.

$$Percentage\ error\ (\%)\ = \frac{(|Threshold\ value - Ground\ truth\ value|)}{Ground\ truth\ value} \quad \textbf{(5)}$$

Meanwhile, in evaluating the overall combined magnification of the similar sample, the average sample porosity was measured through the sum of all the foreground pixels across all the magnifications over the total images that comprised the sample. Since each sample consists of five different magnifications and the resolution of the images is 817 × 567, the porosity formula to measure the average sample porosity was shown in **Eq. (6)**, where *i* is the sample's foreground pixels at different magnifications.

$$overall\ average\ sample\ porosity = \frac{\sum_{i=1}^{n} Foreground\ pixels_i}{5\ (817\ \times\ 567)} \times 100\% \quad \textbf{(6)}$$

In measuring the overall average pore diameter of the samples, the calculation followed as the previous **Eq. (3)** and **Eq. (4)**. The addition of each pore diameter in each magnification was summed up together with the respective physical length into a single dataset. The procedure was done in MS. Excel, and the overall length was average across all measurements. The overall average pore diameter of the samples from three thresholding methods was then compared with the ground truth, and the percentage overall average pore diameter was measured using **Eq. (5)**.

Results and Discussion

Four undoped GaN samples, denoted as U45, U60, U75, and U90, were analyzed. The prefix 'U' in the sample refers to undoped GaN, while the number indicates the respective etching duration in minutes (45, 60, 75, and 90 minutes). The detailed results are summarized in **Table 5**, and a clearer representation of the trend of percentage region error is provided in **Figure 8**. Among the samples, manual thresholding performed relatively better at the shorter etching

International Journal of Innovation and Industrial Revolution
IJIREV
EISSN: 2637-0972
Volume 7 Issue 23 (December 2025) PP. 568-593
DOI 10.35631/IJIREV.723038

duration sample of U45, with an error as low as 22.88% compared to other thresholds. However, the performance deteriorated with increasing porosity as seen in U75 and U90, where errors reached nearly 95%. Otsu thresholding, on the other hand, consistently produces lower errors at longer etching duration of U90, with values of percentage error ranging from 9.29% to 44.62% compared to manual thresholding and adaptive thresholding, which range from 42.11% to 95.60% combined. Nevertheless, as can be seen in U45, the Otsu failed at shorter etching duration where the error exceeded 590% indicating that Otsu is unreliable when pores occupy only a small fraction of the region. Adaptive thresholding generally produced intermediate results by avoiding extreme estimates like Otsu, but did not outperform manual thresholding at low porosity or Otsu at low magnifications.

Table 5: Results Of Porosity and Corresponding Percentage Errors for Otsu, Manual, And Adaptive Thresholding of The Sample Across All Magnifications

Sample	Magnification	Ground Truth Porous Region (%)	Otsu Threshold Porous Region (%)	Manual Threshold Porous Region (%)	Adaptive Threshold Porous Region (%)	Percentage region error (Otsu) (%)	Percentage region error (Manual) (%)	Percentage region error (Adaptive) (%)
U45	25kx	10.75	70.68	2.61	38.82	557.69	75.74	261.27
	50kx	10.55	73.60	4.48	36.44	597.83	57.49	245.52
	100kx	11.80	81.48	4.89	29.87	590.67	58.57	153.23
	200kx	16.87	84.09	20.73	28.08	398.56	22.88	66.51
	250kx	13.11	82.52	19.09	26.25	529.63	45.63	100.29
U60	25kx	41.84	39.54	12.34	37.74	5.51*	70.51	9.81*
	50kx	34.54	40.86	15.32	37.98	18.31*	55.64	9.97*
	100kx	32.78	39.60	18.17	36.19	20.81	44.59	10.39*
	200kx	33.49	45.58	33.41	39.52	36.07	0.25*	18.00*
	250kx	24.82	34.59	32.14	32.20	39.36	29.47	29.72
U75	25kx	60.25	68.53	3.50	37.00	13.74*	94.20	38.58
	50kx	39.88	59.79	4.49	33.79	49.95	88.75	15.25*
	100kx	39.30	64.30	8.50	33.70	63.62	78.38	14.26*
	200kx	77.16	71.92	10.97	25.17	6.79*	85.79	67.38
	250kx	23.50	41.65	18.50	18.65	77.20	21.28	20.66
U90	25kx	65.42	59.34	2.88	32.68	9.29*	95.60	50.05
	50kx	51.27	57.38	3.44	29.68	11.92*	93.29	42.11
	100kx	75.70	54.75	7.62	29.16	27.67	89.93	61.49
	200kx	79.85	54.75	15.89	24.41	31.43	80.10	69.43
	250kx	99.53	55.11	36.91	18.65	44.62	62.92	81.26

International Journal of Innovation and Industrial Revolution
IJIREV
EISSN: 2637-0972
Volume 7 Issue 23 (December 2025) PP. 568-593
DOI 10.35631/IJIREV.723038

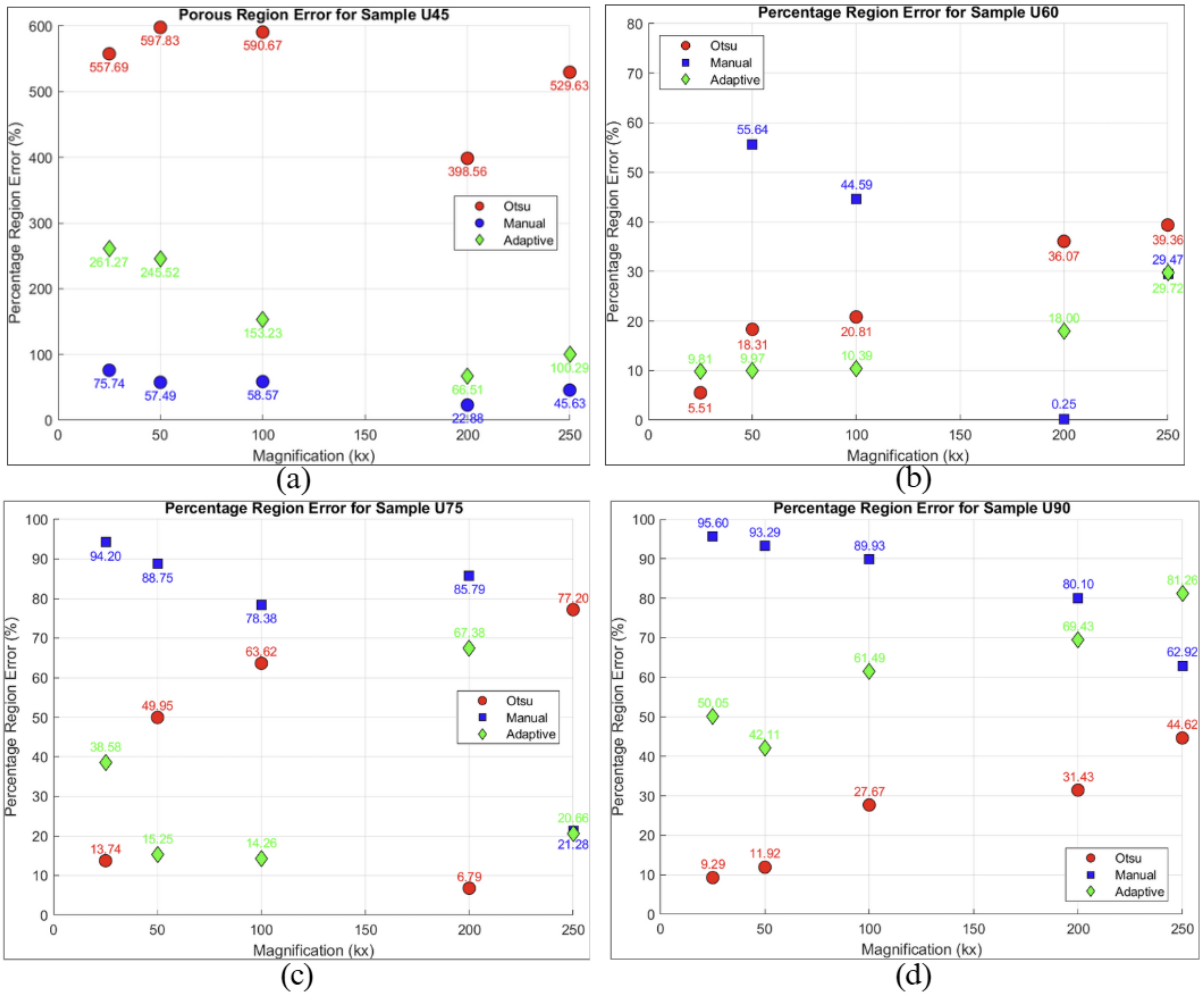

Figure 8: Porous Percentages Region Error Obtained by Otsu Thresholding (Red, Circle), Manual Thresholding (Square, Blue), And Adaptive Thresholding (Green, Diamond) Across Different Magnifications for Samples (A) U45, (B) U60, (C) U75, And (D) U90

These variations across methods emphasize the sensitivity of threshold-based approaches to both porosity level and magnification. In shorter etching duration or low-porosity samples, pixel intensities are largely concentrated within lower-range grayscale values, which highly favors the manual threshold that was preset to 0.2 pixel intensity in segmenting the porous region. Meanwhile, at longer etching durations as in U90, the Otsu thresholding provides a clear separation of porous and surface separation in its pixel intensity toward mid-range grayscale values. This shows the pixel intensity distribution within the U90 is much easier to separate through Otsu. Looking into the trend of magnification, a higher number of estimates with percentage error below 20% were observed at 25kx and 50kx magnification. This can be shown in **Table 5** marked with an asterisk (*), where eight (8) estimates produce close values to the ground truth within this magnification. In contrast, only a limited number of such cases were observed at 100kx and 200kx, but none were observed at 250kx. At a higher magnification of 250kx, the error increased because the enlarged porous structures exhibited shadowy transitions and smoother local variations between porous and surface, making it difficult for Otsu thresholding to assign an optimal separation value. Similar challenges were observed for

International Journal of Innovation and Industrial Revolution
IJIREV
EISSN: 2637-0972
Volume 7 Issue 23 (December 2025) PP. 568-593
DOI 10.35631/IJIREV.723038

manual and adaptive thresholding, underlining the need for more robust approaches when analyzing fine-scale porous structures.

The results of pore diameter estimation and the corresponding percentage errors for each thresholding method are summarized in **Table 6**. For a clearer visualization of the percentage errors in pore diameter estimation, **Figure 9** presents a comparative overview. Across all samples, manual thresholding performed consistently at shorter etching durations as observed in sample U45, which recorded the lowest error of 26.25%. Adaptive thresholding closely followed in a comparable etching trend, showing only a slight difference, with its lowest error observed in a similar sample U45 at 19.36% under 100kx magnification. However, as the etching duration increased, the performance of manual thresholding declined markedly, with errors rising abruptly across all magnifications in U60, U75, and U90, reaching as high as 96.38% in 250kx. At longer etching durations, Otsu thresholding tended to provide the more accurate pore diameter estimation, achieving the lowest error of 0.02% in the U90 sample at 25kx magnification. Nevertheless, Otsu failed to maintain accuracy at higher magnifications across all etching durations. Adaptive thresholding demonstrated competitive performance at lower magnifications, 25kx to 50kx magnification in both U60 and U90, but also exhibited limitations at higher magnifications. The findings in average pore diameter across magnification demonstrate that thresholding performance is influenced by porous morphology and sizes, with manual threshold showing strengths under lower duration etching sample and Otsu at much longer etching duration. In which manual is optimal at any magnification in a lower porosity sample, while Otsu is useful in higher porosity samples but inaccurate at higher magnification. Shifting perspective into the trend of magnification, 25kx and 50kx magnifications exhibited more consistent estimates of average pore diameter, with seven (7) cases showing percentage errors below 20%, as indicated by the asterisk (*) in **Table 6**. Conversely, only three (3) low-error cases were observed at 100kx, and none were recorded at 200kx or 250kx, highlighting the reduced reliability of higher magnifications for pore diameter estimation.

Table 6: Result Of Average Pore Diameter and Corresponding Percentage Errors for Otsu, Manual, And Adaptive Thresholding of The Sample Across All Magnifications

Sample	Magnification	Ground Truth Pore Diameter (nm)	Otsu Threshold Pore Diameter (nm)	Manual Threshold Pore Diameter (nm)	Adaptive Threshold Pore Diameter (nm)	Percentage pore diameter error (Otsu) (%)	Percentage pore diameter error (Manual) (%)	Percentage pore diameter error (Adaptive) (%)
U45	25kx	60.00	89.67	44.25	98.40	49.46	26.25	64.00
	50kx	51.58	88.32	37.08	74.31	71.22	28.11	44.06
	100kx	53.08	110.33	33.51	42.79	107.85	36.87	19.38*
	200kx	49.64	144.31	26.96	25.68	190.69	45.69	48.28
	250kx	45.77	185.34	22.83	23.42	304.97	50.11	48.82
U60	25kx	178.20	105.10	67.74	103.43	41.02	61.99	41.96
	50kx	98.74	69.23	55.91	66.66	29.89	43.38	32.49
	100kx	80.20	45.69	47.35	36.64	43.03	40.95	54.31
	200kx	58.88	27.65	36.06	22.70	53.05	38.76	61.44
	250kx	59.28	18.26	17.09	14.99	69.19	71.18	74.72
U75	25kx	69.40	97.76	58.24	95.32	40.87	16.08*	37.35
	50kx	57.62	64.39	40.85	67.10	11.75*	29.11	16.45*

International Journal of Innovation and Industrial Revolution
IJIREV
EISSN: 2637-0972
Volume 7 Issue 23 (December 2025) PP. 568-593
DOI 10.35631/IJIREV.723038

	100kx	58.49	52.73	34.56	49.27	9.85*	40.91	15.77*
	200kx	111.39	36.50	26.33	22.57	67.23	76.36	79.74
	250kx	45.22	18.43	22.18	14.03	59.25	50.95	68.96
	25kx	84.47	84.45	53.25	87.70	0.02*	36.96	3.83*
	50kx	68.80	73.02	44.55	64.57	6.13*	35.24	6.15*
U90	100kx	109.38	64.81	34.39	37.48	40.75	68.56	65.73
	200kx	180.94	45.97	25.62	19.32	74.60	85.84	89.32
	250kx	418.70	21.45	15.14	12.27	94.88	96.38	97.07

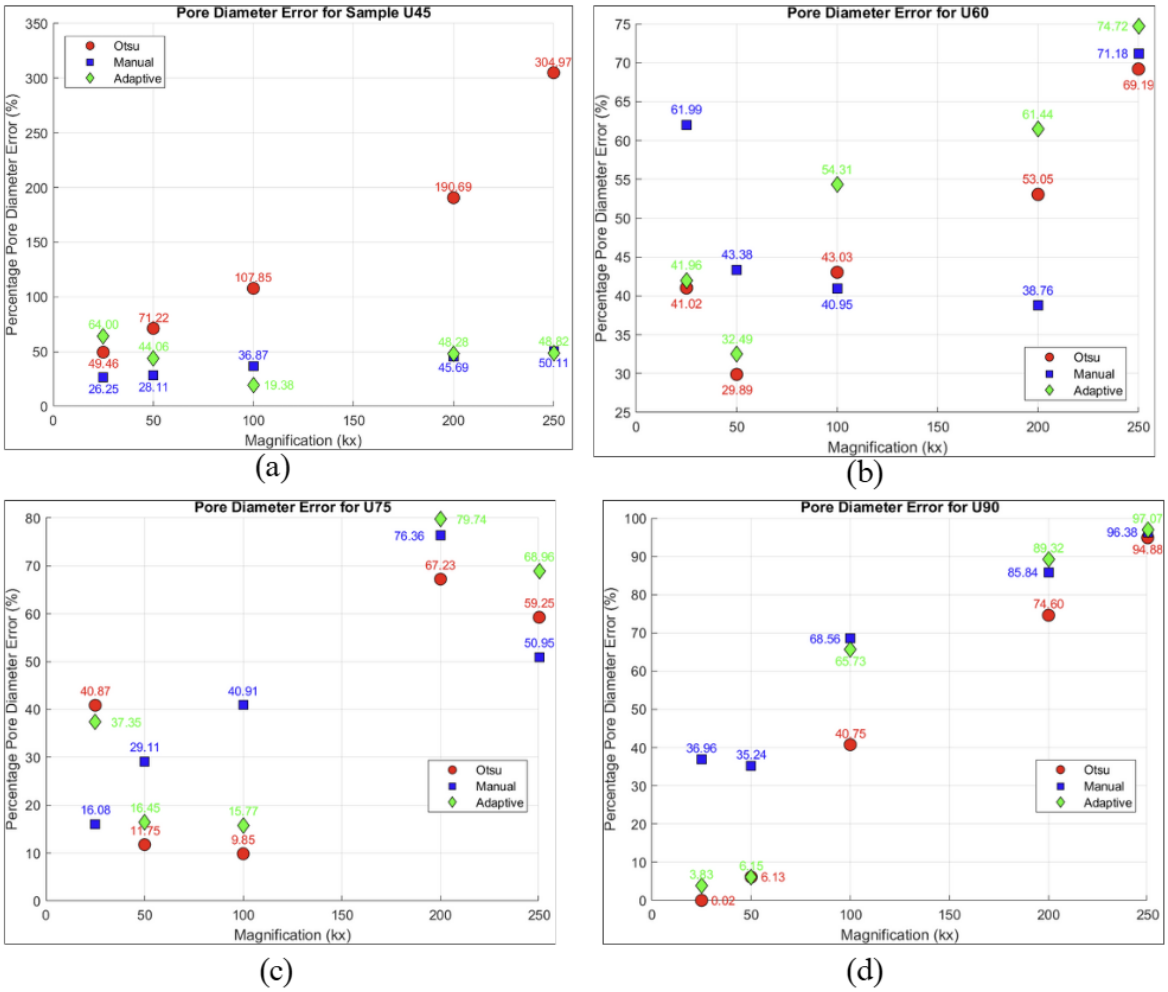

Figure 9: Pore Diameter Error Obtained by Otsu Thresholding (Red, Circle), Manual Thresholding (Square, Blue) And Adaptive Thresholding (Green, Diamond) Across Different Magnifications for Samples (A) U45, (B) U60, (C) U75 And (D) U90

To simplify the analysis and provide an overall perspective, metrics from all magnifications were combined for each sample. This approach enables evaluation of each sample's pore characteristics as a whole, smoothing out magnification-dependent variations and facilitating comparison of thresholding methods. The overall average sample porosity and corresponding percentage region errors for different thresholding methods are presented in **Table 7** and visualized in **Figure 10**.

International Journal of Innovation and Industrial Revolution
IJIREV
EISSN: 2637-0972
Volume 7 Issue 23 (December 2025) PP. 568-593
DOI 10.35631/IJIREV.723038

Table 7: Result Of Overall Average Porosity and Corresponding Percentage Errors for Otsu, Manual and Adaptive Thresholding Methods Across All Samples.

Sample	Average Sample Porosity (%)	Otsu Threshold Average Sample Porosity (%)	Manual Threshold Average Sample Porosity (%)	Adaptive Threshold Average Sample Porosity (%)	Percentage region error (Otsu) (%)	Percentage region error (Manual) (%)	Percentage region error (Adaptive) (%)
U45	12.61	78.48	10.36	31.90	522.18	17.87	152.88
U60	33.50	40.03	22.28	36.73	19.52	33.50	9.64
U75	48.02	61.24	9.19	29.66	27.53	80.86	38.23
U90	74.35	56.27	13.35	26.91	24.32	82.05	63.80

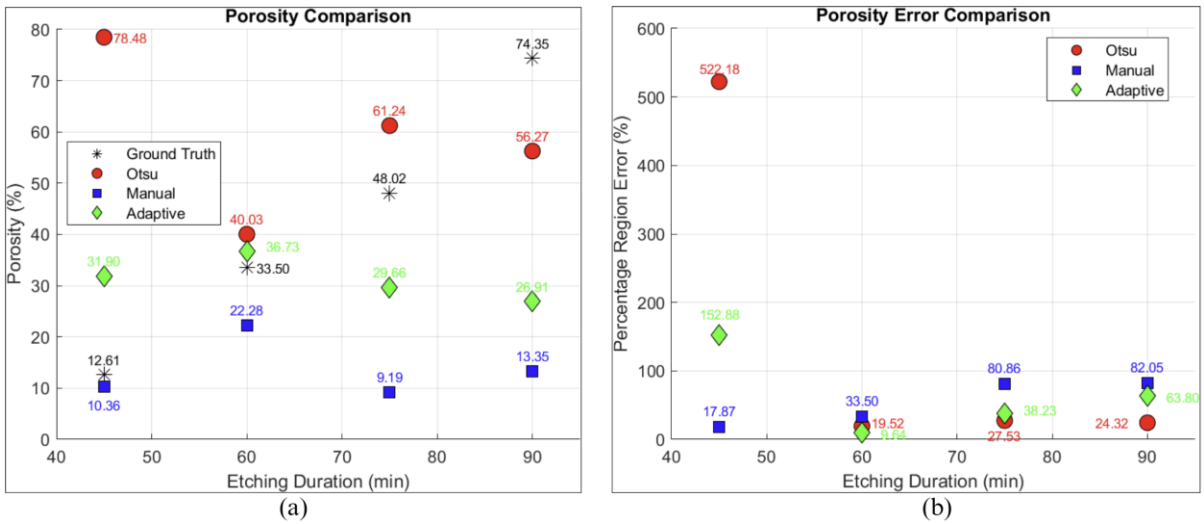

(a) (b)

Figure 10: Comparison Between Thresholding Methods Across All Samples For (A) Average Sample Porosity And (B) Percentage Region Errors.

The results indicate that manual thresholding performs closest to the ground truth at shorter etching durations, with porosity errors as low as 17.87% for U45. However, its accuracy decreases significantly as etching duration increases with the highest porosity error of 82.05%. This highlights that the manual thresholding is less suitable for high porosity sample analysis. For the etching sample of U60, adaptive thresholding exhibits the lowest porosity error among all methods across all samples at 9.64%. At higher etching durations for example, in U75 and U90, adaptive thresholding becomes less accurate, whereas Otsu thresholding achieves relatively lower percentage errors of 27.53% and 24.32%, respectively. These observations suggest that thresholding performance is strongly influenced by etching duration, with manual thresholding favored for shorter durations, adaptive thresholding performing best at moderate durations and Otsu thresholding offering advantages at longer durations.

Next, the overall average pore diameter and corresponding percentage errors for different thresholding methods are summarized in **Table 8** and are visualized in **Figure 11**. The results indicate that thresholding performance varies with etching duration. For the shortest etching

International Journal of Innovation and Industrial Revolution
IJIREV
EISSN: 2637-0972
Volume 7 Issue 23 (December 2025) PP. 568-593
DOI 10.35631/IJIREV.723038

duration in U45, manual and adaptive thresholding yielded almost similar errors with approximately ~32%, while Otsu exhibited a much higher error of 63.33%. This result is consistent with the previous porosity result, whereby at lower etching duration, the manual threshold performed optimally for a less formed porous structure. At etching durations of U60, Otsu thresholding showed the lowest error of 39.41%, compared to manual with 56.20% and adaptive with 46.87%. And again, in the longer etching duration of U75 and U90, Otsu achieved the lowest error with 2.76% and 11.47% respectively. The reason for the low error in higher porosity from Otsu is due to good class separation among the pixel intensity, whereby in the lower porosity sample Otsu was unable to effectively differentiate accurately among the pixel intensity through class variant similar to local mean in the adaptive thresholding. In lower porosity, due to the majority of the porous region dominating the pixel intensity below 0.2, this favors the performance of manual thresholding, leading to a lower percentage error. Overall, the trend indicates that manual thresholding provides pore diameter estimates closest to the ground truth at shorter etching durations, whereas Otsu thresholding yields more accurate estimates at longer etching durations.

Table 8: Overall Average Pore Diameter and Corresponding Percentage Errors for Otsu, Manual, And Adaptive Thresholding Methods Across All Samples.

Sample	Ground Truth Overall Average Pore Diameter (nm)	Otsu Threshold Overall Average Pore Diameter (nm)	Manual Threshold Overall Average Pore Diameter (nm)	Adaptive Threshold Overall Average Pore Diameter (nm)	Percentage pore diameter error (Otsu) (%)	Percentage pore diameter error (Manual) (%)	Percentage pore diameter error (Adaptive) (%)
U45	57.32	93.62	38.90	75.89	63.33	32.13	32.40
U60	134.22	81.32	58.79	71.32	39.41	56.20	46.87
U75	64.23	66.00	45.56	68.05	2.76	29.07	5.94
U90	82.58	73.11	42.04	64.13	11.47	49.09	22.35

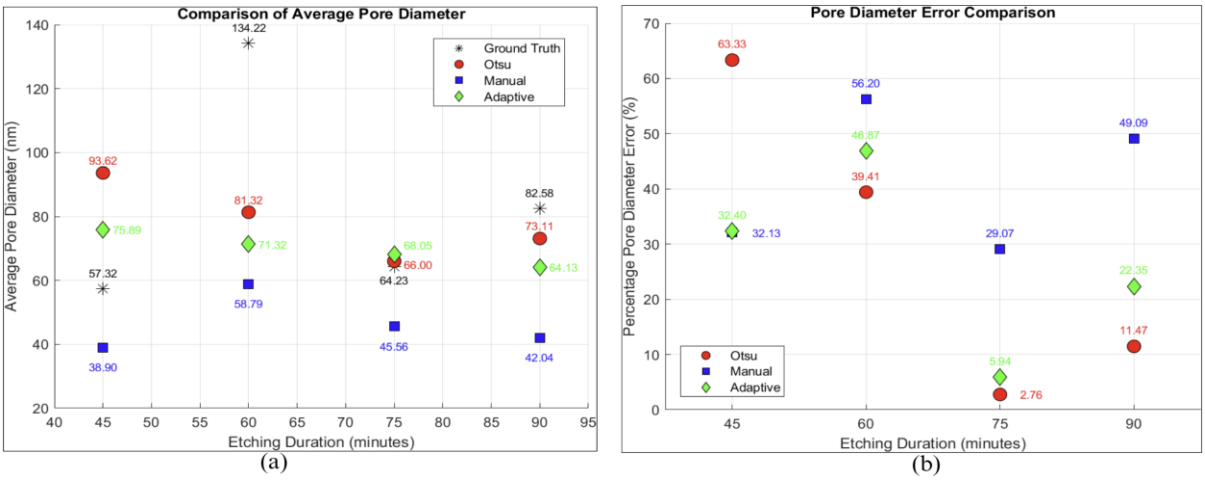

Figure 11: Comparison Between Thresholding Methods Across All Samples For (A) Average Pore Diameter And (B) Pore Diameter Error.

International Journal of Innovation and Industrial Revolution
IJIREV
EISSN: 2637-0972
Volume 7 Issue 23 (December 2025) PP. 568-593
DOI 10.35631/IJIREV.723038

The comparative study of different thresholding techniques for segmenting porous GaN suggests that a mixed thresholding approach could be useful for analyzing porous morphology. Manual thresholding appears more suitable for samples with shorter etching durations, whereas Otsu performs better in higher-porosity samples with longer etching. Nevertheless, further investigation is required to fully understand the influence of magnification across all images. No clear trend could be identified in determining which thresholding method performed best across magnifications. This indicates that threshold appropriateness is highly dependent on both the pixel intensity of the porous region and magnification. Additionally, the difficulty may arise from potential bias introduced during regional selection at higher magnifications, where the field of view often becomes concentrated on pore-rich areas. Localized emphasis of porous structure can exaggerate porosity features, making consistent thresholding and accurate quantification more challenging. These limitations highlight the need for more advanced segmentation techniques to handle the difficulty in smooth contrast transition between the surface and porous region within different magnification procedures.

Conclusion

In this study, 20 FESEM images of porous GaN nanostructure have been analyzed through three different thresholding techniques and have been revealed to produce different porous parameters with respect to the duration and magnification. The analysis has strongly shown that different usage of the thresholding type produces different porous parameter results, with manual thresholding has been shown to be more accurate at lower porosity, while Otsu thresholding at higher porosity samples or longer etching. For example, at lower porosity samples, manual thresholding produced a substantially lower percentage region error of 17.87% compared to Otsu thresholding with 522.18% and adaptive thresholding with 152.88%. A similar trend was observed for average pore diameter estimation, where manual thresholding showed the lowest error of 32.13% while the Otsu thresholding and adaptive thresholding produced 63.33% and 32.40% error. In contrast, for higher porosity samples, the percentage region error for Otsu thresholding is lower at 24.42% compared to manual thresholding with 82.05% and adaptive with 63.80%. A similar can be seen in the percentage average pore diameter error, whereby the Otsu thresholding has a lower percentage error of 11.47% compared to manual thresholding with 49.09% and adaptive thresholding with 22.35%. Furthermore, among the reliable estimates across magnification were found in 25kx and 50kx magnification images. Eight (8) and seven (7) cases showed lower than 20% percentage error in estimating the region and pore diameter at these two magnifications. In contrast, only a limited number of such cases were observed at 100kx and 200kx, and none were observed at 250kx. Challenges to segment porous structures at higher magnification persist, due to shadowy transition and smooth dark local variation, making all thresholding methods used in the study unable to select an optimal separation value. This led to a higher percentage error for estimating the porous region and measuring the average pore diameter at this magnification. The study would like to suggest the use of advanced segmentation techniques that implement a deep learning model to handle the challenges in recognizing the complex pattern of porous structure beyond the greyscale intensities. Semantic or instance segmentation utilizing Mask R-CNN or YOLOv8 architectures should provide a promising alternative to improve the porous parameter quantification when integrated into the image processing workflow used in this study.

International Journal of Innovation and Industrial Revolution
EISSN: 2637-0972 IJIREV
Volume 7 Issue 23 (December 2025) PP. 568-593
DOI 10.35631/IJIREV.723038

Acknowledgements

The authors acknowledge and express their gratitude to the Ministry of Higher Education (MOHE) through the Fundamental Research Grant Scheme (FRGS/1/2022/STG07/UITM/02/1) and MyBrain 2.0 for funding the research project. Additionally, special thanks to UiTM Institute of Postgraduate Studies' Conference Support Funds (100-IPSiS (9/11/8)) for providing financial support for the DASAT2025 conference. Appreciation also extended to Universiti Teknologi MARA Cawangan Pulau Pinang for respective contributions of support and access to workstation facilities. Special thanks to Nur Iwani Nor Izaham for providing the image used in this analysis.

References

Abbas, I. A., & Kadhm, A. J. (2024). Study the Structural Properties of Porous Silicon and their Applications as Thermal Sensors. *Baghdad Science Journal*, *21*(3), 1086–1094. https://doi.org/10.21123/bsj.2023.4097

Abdul Amir, H. A. A., Fakhri, M. A., & Abdulkhaleq Alwahib, A. (2021). Review of GaN optical device characteristics, applications, and optical analysis technology. *Materials Today: Proceedings*, *42*, 2815–2821. https://doi.org/10.1016/j.matpr.2020.12.727

Abdulkhaleq, N. A., Hasan, A. K., & Nayef, U. M. (2020). Enhancement of photodetectors devices for silicon nanostructure from study effect of etching time by photoelectrochemical etching technique. *Optik*, *206*. https://doi.org/10.1016/j.ijleo.2020.164325

Ahmed, N. M., Ramizy, A., Hassan, Z., Amer, A., Omar, K., Al-Douri, Y., & Alattas, O. S. (2012). Nano and micro porous GaN characterization using image processing method. *Optik*, *123*(12), 1074–1078. https://doi.org/10.1016/j.ijleo.2011.07.034

Al-Heuseen, K., & Alquran, M. K. (2018). Stress Relaxation in Porous GaN Prepared by UV Assisted Electrochemical Etching. *IOP Conference Series: Materials Science and Engineering*, *305*(1), 012015. https://doi.org/10.1088/1757-899X/305/1/012015

Cao, Q., Qingge, L., & Yang, P. (2021). Performance Analysis of Otsu-Based Thresholding Algorithms: A Comparative Study. In *Journal of Sensors*. Hindawi Limited. https://doi.org/10.1155/2021/4896853

Cui, J., Zhou, J., Chen, H., & Xiao, H. (2021). Effect of ultraviolet and room lights on porous GaN films using photo-assisted electrochemical etching. *Materials Letters*, *301*. https://doi.org/10.1016/j.matlet.2021.130287

Elia, P., Nativ-Roth, E., Zeiri, Y., & Porat, Z. (2016). Determination of the average pore-size and total porosity in porous silicon layers by image processing of SEM micrographs. *Microporous and Mesoporous Materials*, *225*, 465–471. https://doi.org/10.1016/j.micromeso.2016.01.007

Fauzi, N. A., Isa, I. S., Isa, S. M., Manaf, A. A., Rahim, A. F. A., Mahmood, A., & Noordin, I. R. M. (2023). Gallium Nitride Depth Porosity Using Image Processing Method. In *2023 IEEE 13th Symposium on Computer Applications & Industrial Electronics (ISCAIE)* (pp. 198–202). https://doi.org/10.1109/iscaie57739.2023.10165126

Ge, X., Yin, X., Zeng, Q., Feng, Q., Wang, X., Li, Q., Chen, Z., & Li, C. (2022). Study of dry etched N-polar (Al)GaN surfaces obtained by inductively coupled plasma etching. *Frontiers in Physics*, *10*. https://doi.org/10.3389/fphy.2022.1042998

Hu, T., Zhao, L., Wang, Y., Lin, H., Xie, S., Hu, Y., Liu, C., Zhu, W., Wei, Z., Liu, J., & Wang, K. (2023). High-Sensitivity and Fast-Speed UV Photodetectors Based on Asymmetric

International Journal of Innovation and Industrial Revolution
IJIREV
EISSN: 2637-0972
Volume 7 Issue 23 (December 2025) PP. 568-593
DOI 10.35631/IJIREV.723038

Nanoporous-GaN/Graphene Vertical Junction. *ACS Nano*, *17*(9), 8411–8419. https://doi.org/10.1021/acsnano.3c00263

Hussain, A. A., Mahal, S. H., & Ismael, B. S. (2024). Segmentation and Isolation of Brain Tumors Using Different Images Segmentation Methods. *Baghdad Science Journal*, *21*(8), 2714–2721. https://doi.org/10.21123/bsj.2024.7640

Isa, I. S., Isa, S. M., Abd Manaf, A., Abd Rahim, A. F., Mahmood, A., Abdullah, M. H., & Ad Fauzi, N. (2022). Morphological and structural characteristics of Gallium Nitride (GaN) porosity using image processing. *Optik*, *271*. https://doi.org/10.1016/j.ijleo.2022.170126

Khudiar, S., Nayef, U., & Mutlak, F. (2022). Preparation and Characterization of Porous Silicon for Photodetector Applications. *Journal of Applied Sciences and Nanotechnology*, *2*(2), 64–69. https://doi.org/10.53293/jasn.2021.3646.1032

Kuntyi, O., Zozulya, G., & Shepida, M. (2022). Porous Silicon Formation by Electrochemical Etching. In *Advances in Materials Science and Engineering* (Vol. 2022). Hindawi Limited. https://doi.org/10.1155/2022/1482877

Li, X., Zhai, X., Zhang, Y., Zhang, M., & Tang, J. (2023). A novel mild etchant for photoelectrochemical etching of GaN with enhanced photoresponse. *Materials Letters*, *353*. https://doi.org/10.1016/j.matlet.2023.135226

Mahmood, A., Mahmoud Ahmed, N., Fong Kwong, Y., Lee Siang, C., Bukhari Md Yunus, M., & Hassan, Z. (2014). Applications of the image processing method on the structure measurements in porous GaN. *Journal of Experimental Nanoscience*, *9*(1), 87–95. https://doi.org/10.1080/17458080.2013.814173

Meyers, V., Rocco, E., Hogan, K., Tozier, S., McEwen, B., Mahaboob, I., & Shahedipour-Sandvik, F. (2020). Removal of Dry-Etch-Induced Surface Layer Damage from p-GaN by Photoelectrochemical Etching. *Journal of Electronic Materials*, *49*(6), 3481–3489. https://doi.org/10.1007/s11664-020-07986-2

Muhamad Rizal, M. razali, Nazatul Sabariah Ahmad, Zulkifly Mohd Zaki, & Waidah Ismail. (2014). Region Of Adaptive Threshold Segmentation Between Mean, Median And Otsu Threshold for Dental Age Assessment. *2014 IEEE 2014 International Conference on Computer, Communication, and Control Technology (I4CT 2014)*, 480.

Nor Izaham, N. I., Mahmood, A., Abd Rahim, A. F., Mukhtar, N. M. A., Johan Ooi, M. D., & Ahmed, N. M. (2024). The characterization of nanostructured GaN prepared via low temperature photoelectrochemical etching at different etching period. *Journal of Electrical and Electronic Systems Research (JEESR)*, *25*(1), 108–112. https://jeesr.uitm.edu.my/v1/JEESR/Vol.25/article12.pdf

Quah, H. J., Ahmed, N. M., Hassan, Z., & Lim, W. F. (2016). Surface Alteration of Planar P-Type Gallium Nitride to Porous Structure Using 50 Hz Alternating Current-Assisted Photo-Electrochemical Etching Route. *Journal of The Electrochemical Society*, *163*(8), H642–H651. https://doi.org/10.1149/2.0361608JES/XML

Raheem, K. R., & Shabat, H. A. (2023). An Otsu thresholding for images based on a nature-inspired optimization algorithm. *Indonesian Journal of Electrical Engineering and Computer Science*, *31*(2), 933–944. https://doi.org/10.11591/ijeecs.v31.i2.pp933-944

Son, H., Uthirakumar, P., Polyakov, A. Y., Park, J. H., Lee, K. H., & Lee, I.-H. (2022). Impact of porosity on the structural and optoelectronic properties of nanoporous GaN double layer fabricated via combined electrochemical and photoelectrochemical etching. *Applied Surface Science*, *592*. https://doi.org/10.1016/j.apsusc.2022.153248

International Journal of Innovation and Industrial Revolution
IJIREV
EISSN: 2637-0972
Volume 7 Issue 23 (December 2025) PP. 568-593
DOI 10.35631/IJIREV.723038

Taufiq, S., Syed Nasiruddin, A., Mahmood, A., Maizatul, N., Mukhtar, A., Dayana, M., Ooi, J., Razak, A., Wahab, A., & Syed, T. A. S. N. (2025). Porous GaN fabrication: A bibliometric exploration of electroless, electrochemical and photoelectrochemical etching. *International Journal of Innovation and Industrial Revolution (IJIREV)*, *7*(21), 73–99. https://doi.org/10.35631/IJIREV.721005

Toguchi, M., Miwa, K., Horikiri, F., Fukuhara, N., Narita, Y., Yoshida, T., & Sato, T. (2019). Electrodeless photo-assisted electrochemical etching of GaN using a H3PO4-based solution containing S2O82– ions. *Applied Physics Express*, *12*(6), 066504. https://doi.org/10.7567/1882-0786/AB21A1

Trichas, E., Xenogianni, C., Kayambaki, M., Tsotsis, P., Iliopoulos, E., Pelekanos, N. T., & Savvidis, P. G. (2008). Selective photochemical etching of GaN films and laser lift-off for microcavity fabrication. *Physica Status Solidi (a)*, *205*(11), 2509–2512. https://doi.org/10.1002/PSSA.200780215